Karakoc, Alp; Freund, Jouni

Experimental studies on mechanical properties of cellular structures using Nomex honeycomb cores

Published in:
Composite Structures

Published: 01/01/2012

Document Version
Peer-reviewed accepted author manuscript, also known as Final accepted manuscript or Post-print

Please cite the original version:
Karakoc, A., & Freund, J. (2012). Experimental studies on mechanical properties of cellular structures using Nomex honeycomb cores. *Composite Structures*, (94), 2017-2024.

Experimental studies on mechanical properties of cellular structures using Nomex® honeycomb cores

Alp Karakoç*, Jouni Freund

Aalto University, School of Engineering, Department of Applied Mechanics, P.O.BOX 14300, FI-00076 AALTO, FINLAND

Abstract

An experimental method is presented to obtain the effective in-plane compliance matrices of cellular structures using Nomex® honeycomb cores without a priori assumptions such as orthotropy, etc. In this method, firstly, uni-axial tension tests are carried out for different material orientations. The independent variables in these experiments are the material orientation and displacement of the actuator, while the main dependent variables are positions of the marker points and the force acting on the specimens. Marker tracking technique is used to determine the marker positions which are processed to get strain of the measuring domain, while the stress is estimated through external loading and core geometry. The analysis is confined to the measuring domain under near homogeneous stress and strain fields. The experiment results are processed with transformation and least squares functions to obtain all effective in-plane elastic parameters, which are compared with analytical solution based on deformation of idealized cell structure. Through this comparison, the effects of geometrical parameters of cell structure are discussed in detail. By means of the introduced method, the problem of lack of experimental studies on the effective in-plane compliances of cellular structures in the literature is expected to be solved.

Keywords: Experiment, compliance, Nomex®, honeycomb core, stress, strain

*Corresponding author. Tel.: +358 470 23442.
Email address: alp.karakoc@aalto.fi (Alp Karakoç)

1. Introduction

Honeycomb cores are extensively used in different structural applications such as aviation and automotive industries due to their high stiffness-to-weight ratios. Various analytical techniques and numerical analysis methods have been developed in order to predict in- and out-of-plane mechanical properties of these structures. In many analytical studies, predictions of in-plane core properties have been limited to the assumptions of regular geometry and constant mechanical properties. The approaches are mainly based on bending deformation of inclined walls of a hexagonal unit cell modeled as fixed end-guided end beam [1, 2], while the axial deformation of the vertical walls is neglected due to its minor effect on slender honeycomb cell walls [3, 4]. The studies related to in- and out-of-plane geometrical variations such as core thickness are also available in literature [5, 6]. In contrast to abundance of analytical approaches, there have been very few experimental studies observing the deformation and predicting the material behavior. Schwingschakl et al. [7] made a broad investigation on fifteen analytical approaches and proposed an alternative dynamic experimental method based on resonance response frequencies. Balawi et al. [8] conducted series of uni-axial tension tests in order to understand the effect of relative densities on in-plane elastic moduli of core structures. Despite these efforts, almost no experimental investigations have been performed to calculate all effective in-plane elastic parameters. The main reason is that the experimental calculations, especially for in-plane shear modulus, require either more complicated setup than uni-axial tension test setup or a very clever approach. However, in order to understand the deformation of cellular solids, the experiments on in-plane properties have great importance.

In order to complete this missing link in the literature, an experimental method for the effective in-plane compliances of cellular structures is introduced by testing Nomex® honeycomb cores without a priori assumptions such as orthotropy, periodicity, etc.. In order to understand the mechanical behavior, uni-axial tension tests are carried out for different material orientations and positions of the marker points on the material are precisely measured through the presented marker tracking technique. These data are processed to get strain of the measuring domain as function of stress and thereby the compliance matrix describing the elastic properties of material. Analysis is confined to a measuring domain under near homogeneous stress and strain fields. Experimental results are further compared to analytical results based on an idealized cell structure. This comparison gives opportunity to investigate the effects of the geometrical parameters such as cell wall length, thickness, and corner angle on the effective in-plane elastic parameters.

The present study is expected to advance the current state of the art through simplicity and low cost of the experiment setup, the measurement and analysis techniques, and the applicability of the introduced method to wide range of cellular structures such as honeycomb cores and wood species.

2. Material and Methodology

2.1. Material

Experiments are carried out for Nomex® honeycomb cores with thin cell walls, which are produced from aramid fiber based Nomex® paper dipped in phenolic resin. Its mechanical behavior arises from both the nature of cell wall material and manufacturing process of the core structure. It is known that the cell wall material, Nomex® paper, is produced from fibers aligned in the direction of travel of the paper machine. Thus, it has anisotropy defined with machine and cross (-machine) directions [9]. Besides this characteristic, as shown in Fig. 1, manufacturing of the core structure using corrugation and expansion processes results in directional dependence of mechanical properties [10].

——Preferred position for Fig. 1——

2.2. Theoretical background for in-plane compliance analysis

In order to calculate the effective in-plane mechanical properties of honeycomb cores, various analytical studies have been conducted in which the main strategy comprises core modeling and homogenization [2, 8]. Cell geometry is usually described in terms of cell wall thickness t, wall height h, wall length l and corner angle θ as shown in Fig. 2, whereas cell deformation is based on single cell wall deformation as a consequence of bending, shear and/or axial loading. This mechanism is well described with the beam models and suitable boundary conditions. Thereafter, the effective properties are determined through the behavior of regular cell collection [12].

——Preferred position for Fig. 2——

According to [5], the analytical compliance matrix $[\underline{\mathbf{C}}]$ of honeycomb cores with double thickness vertical walls based on bending deformation can be expressed as

$$[\underline{\mathbf{C}}] = \frac{l^3}{E_s t^3} \begin{bmatrix} \dfrac{\sin^2\theta\,(h/l + \sin\theta)}{\cos\theta} & -\cos\theta\sin\theta & 0 \\ -\cos\theta\sin\theta & \dfrac{\cos^3\theta}{(h/l + \sin\theta)} & 0 \\ 0 & 0 & \dfrac{\cos\theta\,(h^3 + 4h^2 l)}{4\,(hl^2 + l^3\sin\theta)} \end{bmatrix} \tag{1}$$

in which E_s is the cell wall elastic modulus. Comparison between Eq. (1) and the compliance matrix for orthotropic materials in planar case

$$[\underline{\mathbf{C}}] = \begin{bmatrix} 1/E_{W} & -\nu_{LW}/E_{L} & 0 \\ -\nu_{WL}/E_{W} & 1/E_{L} & 0 \\ 0 & 0 & 1/G_{WL} \end{bmatrix} \tag{2}$$

gives the effective in-plane elastic parameters in terms of cell geometry and cell wall elastic modulus. In Eq. (2), E_W, E_L, ν_{WL}, ν_{LW}, and G_{WL} are the effective elastic moduli, shear modulus and Poisson's ratios, respectively, for which $\nu_{LW}/E_L = \nu_{WL}/E_W$ [13].

Eq. (1) describes an orthotropic material having two axes of reflection symmetry and, strictly speaking, applies only to idealized material with a regular cellular structure and constant mechanical properties. However, in the authors' opinion, a priori restrictive assumptions like orthotropy, incompressibility etc. should not be used in any material experiments. Instead, the common approach should include the generalized engineering terms and general anisotropic linear elastic materials because the alignment of principal material directions may not initially be known. In this case, the in-plane compliance matrix is

$$[\underline{\mathbf{C}}] = \begin{bmatrix} 1/E_{W} & -\nu_{LW}/E_{L} & \eta_{WL,W}/E_{W} \\ -\nu_{WL}/E_{W} & 1/E_{L} & \eta_{WL,L}/E_{L} \\ \eta_{WL,W}/E_{W} & \eta_{WL,L}/E_{L} & 1/G_{WL} \end{bmatrix} \tag{3}$$

in which $\eta_{WL,W}$ and $\eta_{WL,L}$ are called coefficients of mutual influence by Lekhnitski and are characterizing the coupling between shearing and normal stresses [14]. After obtaining the parameters of Eq. (3), one should analyze $[\underline{\mathbf{C}}]$ posterior to classify the material. For this purpose, different approaches such as eigendecomposition of $[\underline{\mathbf{C}}]$ can be employed [15].

2.3. Theoretical background for experiments

As illustrated in Fig. 3, laboratory XY and material WL Cartesian coordinate systems (hereafter, abbreviated as cs) are used. The first is used to describe the experiment plane in the laboratory environment, whereas the latter is for the principle plane formed on the material sheet with solid and dashed lines.

——Preferred position for Fig. 3——

In XY-cs, the generic linear stress-strain relation for plane stress condition is constructed using the Voigt notation

$$\{\mathbf{e}\} = [\mathbf{C}]\{\mathbf{s}\} \tag{4}$$

because of practical difficulties in using high-order tensors [16]. Curly {} and square brackets [ ] are operators for representing tensors as column vectors and matrices, respectively. In Eq. (4), $\{\mathbf{e}\}$ and $\{\mathbf{s}\}$ are the column vector representations of strain and stress tensors with assumption of symmetry ($e_{ij} = e_{ji}$ and $s_{ij} = s_{ji}$ for $i, j \in \{X, Y\}$), whereas $[\mathbf{C}]$ is the square matrix representation for the fourth-order compliance tensor $\mathbf{C}$. Here, it should be noted that $[\mathbf{C}]$ denotes the compliance in the basis of XY-cs, while $[\underline{\mathbf{C}}]$ is expressed in the basis of WL-cs. Eq. (4) can be expanded to the components as

$$\left\{ \begin{array}{c} e_{XX} \\ e_{YY} \\ 2e_{XY} \end{array} \right\} = \begin{bmatrix} C_1 & C_2 & C_3 \\ C_4 & C_5 & C_6 \\ C_7 & C_8 & C_9 \end{bmatrix} \left\{ \begin{array}{c} s_{XX} \\ s_{YY} \\ s_{XY} \end{array} \right\} \tag{5}$$

involving 9 parameters, some of which may not be independent. As presented in Eq. (3), for a general anisotropic linear elastic material, the number of independent parameters is equal to 6, which is due to the compliance symmetry originated from the strain energy density [17]. For an orthotropic material, which is invariant to reflection with respect to two certain perpendicular axes, there exist 4 independent parameters where the coupling terms such as $\eta_{WL,W}$, $\eta_{WL,L}$ are zeros or in negligible orders [18]. In case of isotropy, where the matrix is invariant to rotation, the number is further reduced to 2. The compliance matrix $[\mathbf{C}]$ of Eq. (5) may well be singular. It is noteworthy that generic notations $\mathbf{e}$, $\mathbf{s}$ are used for the strain and stress tensors which may differ from small strain tensor $\boldsymbol{\epsilon}$ and Cauchy stress tensor $\boldsymbol{\sigma}$, respectively.

Transformation rules for stress and strain components of different basis are given as

$$\left\{ \begin{array}{c} e_{XX} \\ e_{YY} \\ 2e_{XY} \end{array} \right\} = [\mathbf{T}]^{\mathrm{T}} \left\{ \begin{array}{c} e_{WW} \\ e_{LL} \\ 2e_{WL} \end{array} \right\} \tag{6}$$

and

$$\left\{ \begin{array}{c} s_{XX} \\ s_{YY} \\ s_{XY} \end{array} \right\} = [\mathbf{T}]^{-1} \left\{ \begin{array}{c} s_{WW} \\ s_{LL} \\ s_{WL} \end{array} \right\} \tag{7}$$

in which superscripts T, -1 denote the matrix transpose and inverse, respectively. According to [14],

$$[\mathbf{T}] = \left[\begin{array}{ccc} \cos^2\varphi & \sin^2\varphi & \sin 2\varphi \\ \sin^2\varphi & \cos^2\varphi & -\sin 2\varphi \\ -\frac{1}{2}\sin 2\varphi & \frac{1}{2}\sin 2\varphi & \cos 2\varphi \end{array} \right]. \tag{8}$$

where φ is the counterclockwise orientation angle between X- and W-axes, which is demonstrated in Fig. 3.

These transformation rules are used to express $[\mathbf{C}]$ of any rotated coordinate system in terms of $[\underline{\mathbf{C}}]$ in WL -cs. Using Eqs. (5), (6) and (7),

$$\left[\begin{array}{ccc} C_1 & C_2 & C_3 \\ C_4 & C_5 & C_6 \\ C_7 & C_8 & C_9 \end{array} \right] = [\mathbf{T}]^{\mathrm{T}} \left[\begin{array}{ccc} \underline{C}_1 & \underline{C}_2 & \underline{C}_3 \\ \underline{C}_4 & \underline{C}_5 & \underline{C}_6 \\ \underline{C}_7 & \underline{C}_8 & \underline{C}_9 \end{array} \right] [\mathbf{T}]. \tag{9}$$

Therefore, it is enough to measure the compliance in some convenient coordinate systems.

In principle, the values of $\underline{C}_1, .., \underline{C}_9$ can be measured by using a minimum of three linearly independent homogeneous stress states $s^i_{XX}, s^i_{YY}, s^i_{XY}$ $(i = 1, 2, 3)$. Assuming that the corresponding strain components $e^i_{XX}, e^i_{YY}, e^i_{XY}$ are measured in some manner,

$$[\underline{\mathbf{C}}] = \left[\begin{array}{ccc} e^1_{XX} & e^2_{XX} & e^3_{XX} \\ e^1_{YY} & e^2_{YY} & e^3_{YY} \\ e^1_{XY} & e^2_{XY} & e^3_{XY} \end{array} \right] \left[\begin{array}{ccc} s^1_{XX} & s^2_{XX} & s^3_{XX} \\ s^1_{YY} & s^2_{YY} & s^3_{YY} \\ s^1_{XY} & s^2_{XY} & s^3_{XY} \end{array} \right]^{-1}. \tag{10}$$

This equation fulfills the basic requirements to obtain material parameters [19, 20]. However, in order to be more precise, specimens should be tested for more than three orientations relative to loading direction. In this case, the parameters can be calculated as the minimizer of the least squares function

$$\pi(\underline{C}_1, .., \underline{C}_9) = \sum_{i=1}^{n} \left\| \left\{ \begin{array}{c} e^i_{XX} \\ e^i_{YY} \\ e^i_{XY} \end{array} \right\} - \left[\begin{array}{ccc} C_1 & C_2 & C_3 \\ C_4 & C_5 & C_6 \\ C_7 & C_8 & C_9 \end{array} \right] \left\{ \begin{array}{c} s^i_{XX} \\ s^i_{YY} \\ s^i_{XY} \end{array} \right\} \right\|^2 \qquad (11)$$

in which the compliance is given by Eq. (9), the matrix norm $\|\|$ is Euclidean. Use of several angular measurements and repetitions makes it possible to quantify the error in the fit which serves as an indicator in experiment or processing data. For a unique minimizer, i.e. the values of the material parameters, the number of independent equations in Eq. (11) should exceed or be equal to that of the parameters.

3. Experiments on compliance

As illustrated in Fig. 3 and Fig. 4, uni-axial tension tests are conducted on specimens with various orientations relative to loading direction. ASTM C363 test method for sandwich constructions and cores is followed in the specimen preparation and testing stages [21]. The experiments are carried out with several repetitions in order to minimize the random measurement errors. Thereafter, the measured data are processed to get strains of the measuring domains as functions of stresses and thereby the compliance matrices describing the elastic properties of Nomex® honeycomb cores.

——Preferred position for Fig. 4——

3.1. Design of experiments

The experiments are designed in the way that material type, displacement of the hydraulic actuator and specimen orientation angle φ relative to uni-axial load are considered as the independent variables. The material type is described in terms of cell geometry t, h, l, θ, cell wall elastic modulus E_s, and core thickness $\mathcal{T}$. The dependent variables of the experiments are the load vector $\vec{F}$ and position data of the markers in the measurement domain which are used in the stress and strain calculations. Eventually, both stress and strain data are employed in compliance calculations as the final output.

In this section, the independent variables are explained in detail, while the rest is clarified in the following sections.

As listed in Table 1 and presented in Fig. 4, three different cell sizes, which are c_1=5 mm, c_2=6 mm, c_3=13 mm, and two different core thicknesses of $\mathcal{T}_1 = 7$ mm and $\mathcal{T}_2 = 12$ mm are used in order to evaluate the influences of dimensional parameters on the effective in-plane mechanical properties. Samples are formed based on these two parameters, whereas the specimens of each sample are generated using four different orientations $\varphi_1 = 0°$, $\varphi_2 = 90°$ and $\varphi_{3,4} = \pm 45°$ relative to uni-axial loading. In determining the width $\mathcal{W}$ and length $\mathcal{L}$ of specimens, ASTM C363 is taken into consideration. For precision of the measurements, each specimen is tested twice. The accuracy of the results is then sought through the analytical solution in Eq. (1).

——Preferred position for Table 1——

For the comparison of experimental and analytical results in the following sections, the arithmetic means of measured geometrical parameters are tabulated in Table 1. These measurements are taken from various locations of random specimens within each sample; therefore, they represent the general characteristics of samples rather than individual specimens.

3.2. Experiment setup

The experiments are conducted in a steel frame of 920 × 920 mm^2 with wall thickness of 60 mm as shown in Fig. 5. The large frame gives flexibility to test large specimens, which is important to prevent the artifacts due to boundary conditions and provide suitable loading in the measurement domain. The bottom section of the specimen is fixed using fixture plates connected to a stationary joint, whereas the top section is adjusted to move upwards and downwards along an axis. The aforementioned constraints provide proper conditions for uni-axial loading of the specimens.

——Preferred position for Fig. 5——

Actuating system of the setup is designed so that a hydraulic servo cylinder with a pressure up to 16 MPa is driven at the speed of 0.1 mm/s by a signal generator. The duration of the tests varies from 3 to 6 minutes with a constant loading rate. Force is measured through a force transducer with an upper limit of 10 kN, while the displacements of the core structure is measured with displacement transducer. Besides, marker positions in the measurement domain are measured with image capturing and marker tracking technique.

4. Analysis

4.1. Marker tracking

The positions of the markers during the experiment are obtained with marker tracking technique. The advantage of this technique, compared to conventional displacement measurement equipments such as linear variable differential transformer (LVDT), is that there is no need to select the measuring domain beforehand. In this way, the experimenter has higher control for defining the domain, which results in more precise results.

——Preferred position for Fig. 6——

For the marker tracking, an in-house code has been developed and verified with rigid body motion tests. During the experiments, digital images of the domain are captured every 4 seconds in synchronization with loading. Then, each image is converted from RGB to grey-scale image after contrast and brightness adjustments as seen in Fig. 6. This is followed by binary image conversion using a histogram-based threshold method [22]. In binary images, the markers are represented as sets of white pixels and by averaging the positions of these pixels, marker center coordinates (X_i, Y_i) are calculated. This process is repeated for each image frame in order to generate marker position data.

4.2. Displacement analysis

As the first step of displacement calculations, each marker is paired with the closest one in the following image frame by using nearest neighbor query. Then, the marker displacements associated with frame f are obtained as

$$\left\{ \begin{array}{c} u_i^f \\ v_i^f \end{array} \right\} = \left\{ \begin{array}{c} X_i^{f+1} - X_i^f \\ Y_i^{f+1} - Y_i^f \end{array} \right\}. \tag{12}$$

Here, u and v are the displacements along X- and Y-axes, respectively.

The displacements are considered as values of continuous linear displacement field $\vec{u}^f$ which is obtained through the analysis of position data. In component form, it is expressed as

$$\left\{ \begin{array}{c} u^f \\ v^f \end{array} \right\} = \left[\begin{array}{ccc} a_u^f & b_u^f & c_u^f \\ a_v^f & b_v^f & c_v^f \end{array} \right] \left\{ \begin{array}{c} 1 \\ X \\ Y \end{array} \right\}. \tag{13}$$

in which a_u, b_u,.., c_v are the polynomial coefficients. In Eq. (13), higher order polynomials may well be used but the experiments are designed to produce homogeneous strains in the domain. Here, a_u, b_u,.., c_v are the minimizers of least squares function

$$\pi(a_u, b_u, \ldots, c_v) = \sum_{i=1}^{n} \left\| \left\{ \begin{array}{c} u_i^f \\ v_i^f \end{array} \right\} - \left[\begin{array}{ccc} a_u^f & b_u^f & c_u^f \\ a_v^f & b_v^f & c_v^f \end{array} \right] \left\{ \begin{array}{c} 1 \\ X_i^f \\ Y_i^f \end{array} \right\} \right\|^2 \tag{14}$$

in which the sum is over n markers. These coefficients are separately calculated for each frame. Hereafter, superscript f is excluded for simplicity in the notation.

The outcome of displacement analysis is the deformation gradient $\mathbf{F}$. According to [23],

$$[\mathbf{F}] = \left[\begin{array}{cc} 1 + u_{,X} & u_{,Y} \\ v_{,X} & 1 + v_{,Y} \end{array} \right] = \left[\begin{array}{cc} 1 + b_u & c_u \\ b_v & 1 + c_v \end{array} \right] \tag{15}$$

in which $_{,X}$ and $_{,Y}$ are the partial derivative operators.

4.3. Strain measure

For any material body, deformation is decomposed into three operations: translation, rotation and stretch. The first two define rigid body motions, while the latter is used to calculate the strain measure, e.g. the Green-Lagrange strains

$$[\mathbf{E}] = \frac{1}{2}([\mathbf{U}]^2 - [\mathbf{I}]) \tag{16}$$

which is invariant to rotation [24]. Here, $\mathbf{I}$ is identity tensor and $\mathbf{U}$ is the right stretch tensor of which square is given as

$$[\mathbf{U}]^2 = [\mathbf{F}]^{\mathrm{T}}[\mathbf{F}]. \tag{17}$$

As seen in Fig. 7, the deformation due to cell wall bending results in the structural linear elasticity, which also fulfills the small strains $\boldsymbol{\epsilon}$ assumption. Hence, substituting $[\mathbf{U}] = [\boldsymbol{\epsilon}] + [\mathbf{I}]$ in Eq. (16) and omitting the second order term give

$$[\mathbf{E}] = \frac{1}{2}([\mathbf{I}] + 2[\boldsymbol{\epsilon}] + [\boldsymbol{\epsilon}]^2 - [\mathbf{I}]) \approx [\boldsymbol{\epsilon}]. \tag{18}$$

——Preferred position for Fig. 7——

4.4. Stress measure

For the constitutive modeling, the stress measure is selected to be invariant to rotations and symmetric because of the strain measure characteristics in Eqs. (16) and (17). According to [25], these can be satisfied with the first and second Piola-Kirchhoff stress tensors. In order to calculate the first Piola-Kirchhoff stress tensor $\mathbf{P}$, the infinitesimal load vector $d\vec{F}$ in the deformed configuration is directly transferred to the initial configuration based on vector invariance. Then, $\mathbf{P}$ is expressed in terms of $d\vec{F}$, unit area dA and unit surface normals $\vec{N}^1$, $\vec{N}^2$ in the initial configuration as presented in Fig. 8. The components of $\mathbf{P}$ in the basis of XY-cs can be calculated through

$$\begin{Bmatrix} dF^i_X \\ dF^i_Y \end{Bmatrix} = \begin{bmatrix} P_{XX} & P_{YX} \\ P_{XY} & P_{YY} \end{bmatrix} \begin{Bmatrix} N^i_X \\ N^i_Y \end{Bmatrix} dA;\ i \in \{1, 2\}. \tag{19}$$

The calculations are carried out for two unit surfaces of the infinitesimal element in order to solve four unknown components P_{XX}, P_{YY}, P_{YX} and P_{XY}.

However, $\mathbf{P}$ is a two-point tensor and not symmetric, which is not convenient to operate with the symmetric strain tensor $\mathbf{E}$. Instead, the second Piola-Kirchhoff stress tensor $\mathbf{S}$, which is symmetric and energy conjugate to $\mathbf{E}$, is preferred. According to [23], the transformation between $\mathbf{S}$ and $\mathbf{P}$ is given in the matrix form as

$$[\mathbf{S}] = [\mathbf{F}]^{-1}[\mathbf{P}]. \tag{20}$$

Eventually, the components of $\mathbf{S}$ and $\mathbf{E}$ are replaced with $\mathbf{s}$ and $\mathbf{e}$ of Eq. (11) in order to calculate the compliance matrix components as the minimizers of the least squares function.

5. Results and discussions

As observed in Fig. 7, cell wall deformation starts with cell wall bending in the linear elastic region. However, during the later stages of the experiment, densification and other mechanisms start to dominate the deformation, leading to nonlinear elasticity and consequently, cell wall separations. Since the main purpose is to calculate the compliance matrices, the study is limited to small displacements of cell walls under bending mechanism.

——Preferred position for Fig. 7——

The first notable outcomes of these experimental compliances are the coefficients of mutual influence $\eta_{WL,W}$ and $\eta_{WL,L}$ which are used to classify the material. If these are equal to zero in the planar case, material is called as orthotropic, which represents a particular type of anisotropy. As seen in Table 2, $\eta_{WL,W}$ and $\eta_{WL,L}$ are close to zero, which means that the tested honeycomb cores can also be classified as orthotropic materials.

The limitation for the cell wall deformation and material classification posterior to the experiments lead the authors to make a proper comparison between the experimental results and analytical solution in Eq. (1) which is derived based on the same conditions. Through this comparison, the influences of geometrical parameters of cell structures on the effective elastic properties are investigated. Here, it is noteworthy that the cell wall elastic modulus $E_s \approx 7.9$ GPa, which was measured through uni-axial tension tests of unit cell structure beforehand.

In order to understand the effects of the tabulated geometrical parameters in Table 2, the comparisons are classified into two parts: comparisons between samples and the same cell size samples. It is important to underline that three different cell sizes c_1=5 mm, c_2=6 mm, c_3=13 mm and two different core thicknesses $\mathcal{T}_1$=7 and $\mathcal{T}_2$=12 mm have been investigated.

——Preferred position for Table 2——

Comparison between samples of the same thicknesses shows that E_W, E_L, G_{WL} and ν_{LW} have high dependency on the corner angle θ for both $\mathcal{T}_1$=7 and $\mathcal{T}_2$=12 mm, whereas ν_{WL} is less sensitive to θ for $\mathcal{T}_1$=7 mm. As seen in Table 2, E_L, G_{WL} and ν_{LW} are directly proportional to θ; however, E_W and ν_{WL} are inversely proportional. This is mainly related to the contribution of the inclined cell walls [4]. When θ has greater value than 30°, more material is oriented along L-axis. Therefore, material gets stiffer along this axis; on the contrary, softer along W-axis. As a result, there are drastic raises or drops on the in-plane elastic moduli for even small angular changes. On the other hand, it is very difficult to mention about individual effects of the cell wall thickness t and length l. However, their combined effect t/l shows that when t/l decreases, cell walls become more slender and less resistant. As a consequence, all effective in-plane moduli decrease, which has been investigated in literature [2, 3, 4]. The same effect can also be observed through the comparison between samples S-5-7 and S-13-12, which have almost the same corner angles.

Efforts are put into understanding the effect of $\mathcal{T}$ in same cell size sample comparisons. Nevertheless, its effect seems trivial in regard to the dominant effect of cell geometry.

6. Conclusions

In this study, an experimental method is presented for measuring the effective in-plane compliance matrices of cellular structures using Nomex® honeycomb cores. In contrast to previous studies in the literature, a prior assumptions regarding to geometrical and mechanical characterizations are avoided. Instead, general anisotropic linear elastic material relationship in two dimensional space is used and material classification is done based on the measured effective in-plane elastic parameters. Besides the effective in-plane elastic moduli and Poisson's ratios, shear modulus and coefficients of mutual influence characterizing the coupling between shearing and normal stresses are measured. In this respect, the problem of lack of experimental studies on this issue is expected to be solved with the present method.

In order to obtain these effective parameters, uni-axial tension testing of Nomex® honeycomb cores with various material orientations relative to loading direction are carried out in the first step. In these experiments, the data is gathered for small displacement of cell walls under bending mechanism because linear elasticity is taken into consideration. The results are given in terms of the stress and strain measures and processed with transformation and least squares functions. It is noteworthy that measurement errors are tried to be minimized with the proposed marker tracking technique for honeycomb cores in replacement of conventional equipments such as linear variable differential transformer (LVDT), while analysis errors are minimized with several repetitions of the experiments. As a result, the effective in-plane compliances are calculated with the minimum practical error. Analyses of these compliances show that the tested honeycomb cores can be classified as orthotropic materials.

The limitation for the cell wall deformation and material classification posterior to the experiments lead the authors to make a proper comparison between the experimental results and analytical solution which is derived based on the same conditions. For this purpose, firstly, the geometrical parameters of cell structure such as corner angle, wall length and thickness are measured. Then, through the comparison study, the influences of these parameters on the effective in-plane elastic properties are investigated. This study reveals that the corner angle and the ratio of cell wall thickness to length have drastic effects.

The present study provides direct access to all effective parameters and coupling terms by means of the introduced experiment and analysis techniques. Eventually, it is expected to advance the current state of the art through simplicity and low cost of the experiment setup, the measurement and analysis techniques, and the applicability of the method to wide range of cellular structures such as honeycomb cores and wood species.

Acknowledgments

The authors gratefully acknowledge the financial support of Multidisciplinary Institute of Digitalisation and Energy through Energy Efficient Wood Processing and Machining Project (E-wood) and the Ministry of Education of Finland through the National Graduate School in Engineering Mechanics.

References

[1] Roark RJ, Young WC. Formulas for Stress and Strain. New York: McGraw-Hill; 2002.

[2] Gibson LJ, Ashby MF. Cellular solids, structure and properties. Cambridge: Cambridge University Press; 1999.

[3] Masters IG, Evans KE. Models for the elastic deformation of honeycombs. Composite Structures 1996;35:403-422.

[4] Balawi S, Abot JL. A refined model for the effective in-plane elastic moduli of hexagonal honeycombs. Composite Structures 2008;84:147-158.

[5] Chen DH, Horii H, Ozaki S. Analysis of in-plane elastic modulus for a hexagonal honeycomb core: Analysis of Young's modulus and shear modulus. Journal of Computational Science and Technology 2009;3:1-12.

[6] Zhu HX, Hobdell JR, Windle AH. Effects of cell irregularity on the elastic properties of 2D Voronoi honeycombs. Journal of the Mechanics and Physics of Solids 2001;49:857-870.

[7] Schwingschakl CW, Aglietti GS, Cunningham PR. Determination of honeycomb material properties: Existing theories and an alternative dynamic approach. Journal of Aerospace Engineering 2006;19:177-183.

[8] Balawi S, Abot JL. The effect of honeycomb relative density on its effective in-plane elastic moduli: An experimental study. Composite Structures 2008;84:293-299.

[9] Scandinavian Pulp, Paper and Board Testing Committee. Identification of machine and cross directions. Stockholm: ScanP9-93; 1993.

[10] Bitzer T. Honeycomb Technology: Materials, design, manufacturing, applications and testing. Springer; 1997.

[11] Hexcel product data sheet: (Available online: http://www.hexcel.com/Resources/Honeycomb-Data-Sheets (Last check: October 2011))

[12] Xu XF, Qiao P. Homogenized elastic properties of honeycomb sandwich with skin effect. International Journal of Solids and Structures 2002;39:2153-2188.

[13] Itskov M, Aksel N. Elastic constants and their admissible values for incompressible and slightly compressible anisotropic materials. Acta Mechanica 2002;157:91-96.

[14] Jones RM. Mechanics of Composite Materials. Washington, D.C.: McGraw-Hill Book Company; 1975.

[15] Felippa CA, Onate E. Stress, strain and energy splittings for anisotropic elastic solids under volumetric constraints. Computers and Structures 2003;81:1343-1357.

[16] Belytschko T, Liu WK, Moran B. Nonlinear Finite elements for Continua and Structures, 1st Ed. New York: Wiley-Sons; 2000.

[17] Kaw AK. Mechanics of Composite Materials, 2nd Ed. Boca Raton: Taylor-Francis Group; 2006.

[18] Tuttle ME. Structural analysis of polymeric composite materials. New York: Marcel Dekker Inc.; 2003.

[19] Morozov EV, Vasiliev VV. Determination of the shear modulus of orthotropic materials from off-axis tension tests. Composite Structures 2003;62:379-382.

[20] Balawi S. Effective Mechanical Behavior of Honeycombs: Theoretical and Experimental Studies. University of Cincinnati; 2007.

[21] MIL-STD-401B. Military standard sandwich constructions and core materials, general test methods. Department of Defense; 1967.

[22] Sezgin M, Ankur B. Survey over image thresholding techniques and quantitative performance evaluation. Journal of Electronic Imaging 2004;13:146-165.

[23] Gonzalez O, Stuart AM. A First Course in Continuum Mechanics. Cambridge: Cambridge University Press; 2008.

[24] Bazant ZP. Easy-to-compute tensors with symmetric inverse approximating Hencky finite strain and its rate. Journal of Engineering Materials 1998;120:131-136.

[25] Jirasek M, Bazant ZP. Inelastic analysis of structures. Chichester: John Wiley-Sons; 2002.

Table 1: The arithmetic means of measured geometrical parameters. These are measured for all the specimens in each sample denoted with prefix S-. Each sample consists of specimens with orientation angles of $\varphi_1 = 0°$, $\varphi_2 = 90°$ and $\varphi_{3,4} = \pm 45°$ relative to uni-axial loading. The tabulated parameters are represented for clarification in Fig. 4.

Sample	c [mm]	h (~l) [mm]	t [mm]	θ [˚]	$\mathcal{T}$ [mm]	$\mathcal{W}$ [mm]	$\mathcal{L}$ [mm]
S-5-7	5	2.5	0.05	32	7	143	244
S-5-12	5	2.5	0.05	34	12	144	245
S-6-7	6	3.2	0.06	26	7	143	246
S-6-12	6	3.2	0.06	28	12	146	247
S-13-7	13	6.6	0.13	32	7	145	247
S-13-12	13	6.8	0.13	32	12	143	244

Table 2: Comparison between experimental and analytical results. Prefix An- is used for predicted results obtained through analytical solution in Eq. (1).

Sample	l [mm]	t [mm]	θ [°]	E_W [kPa]	E_L [kPa]	G_{WL} [kPa]	ν_{WL}	ν_{LW}	$-\eta_{WL,W}$	$-\eta_{WL,L}$
S-5-7	2.5	0.05	32	121.0	158.5	92.6	1.12	1.47	0.019	-0.103
An-S-5-7				124.1	157.7	90.7	0.89	1.13	---	---
S-5-12	2.5	0.05	34	105.8	159.8	98.3	0.97	1.47	-0.049	0.004
An-S-5-12				106.9	172.0	94.6	0.79	1.27	---	---
S-6-7	3.2	0.06	26	171.9	118.0	64.3	1.31	0.89	-0.048	0.077
An-S-6-7				168.4	102.6	66.3	1.28	0.78	---	---
S-6-12	3.2	0.06	28	150.0	105.7	71.4	1.29	0.91	-0.104	-0.075
An-S-6-12				141.2	110.6	69.0	1.13	0.88	---	---
S-13-7	6.6	0.13	32	122.9	154.2	91.9	1.26	1.58	0.073	-0.069
An-S-13-7				118.5	150.6	86.7	0.88	1.13	---	---
S-13-12	6.8	0.13	32	96.5	128.2	84.6	0.91	1.21	0.004	0.024
An-S-13-12				108.4	137.7	79.2	0.88	1.13	---	---

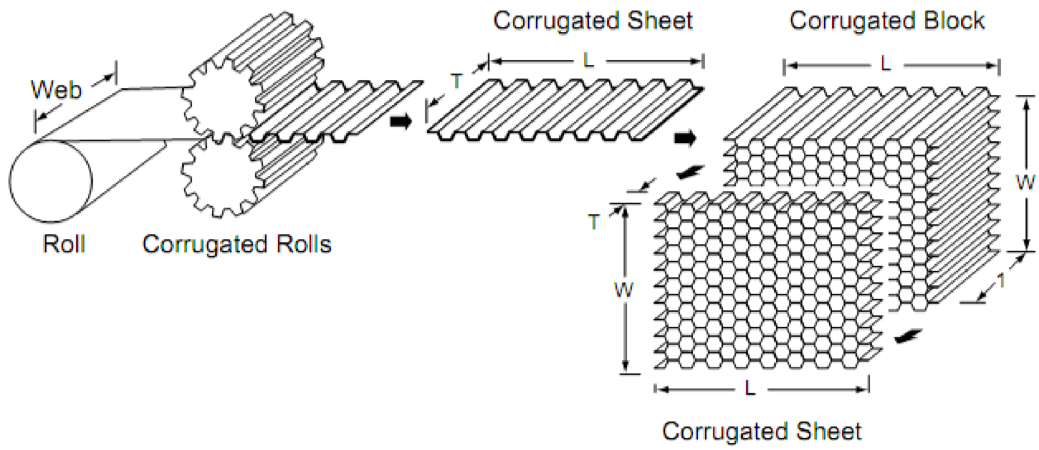

Figure 1: Production process of honeycomb core [11].

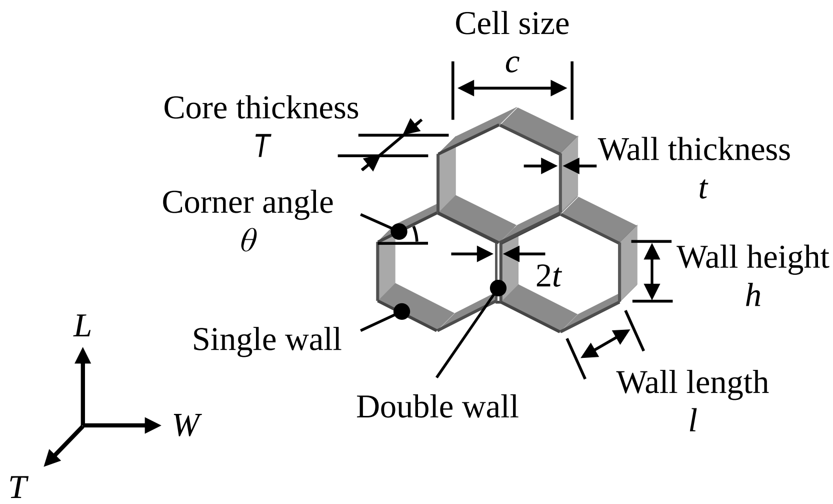

Figure 2: Geometrical parameters for honeycomb cores and cell walls. Here, W, L, T refer to transverse, longitudinal and thickness directions, respectively [2, 11].

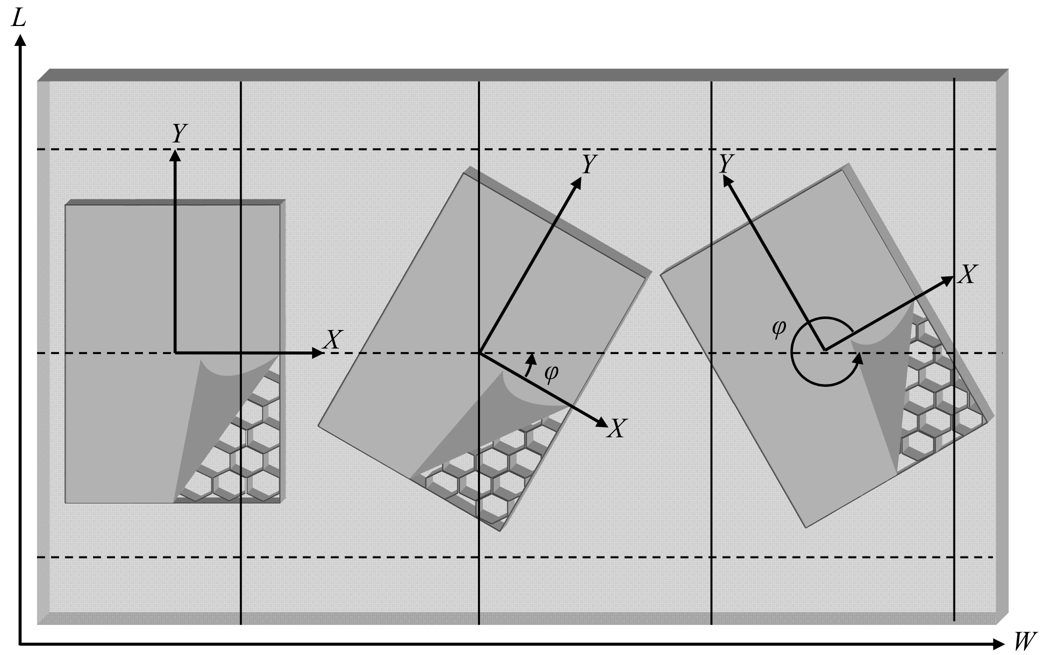

Figure 3: Specimens taken out from the sheet based on predefined angles. The dashed horizontal lines correspond to W-axis, while the solid vertical lines are for L-axis which are drawn on the sheet. Here, φ is the counterclockwise orientation angle between X- and W-axes.

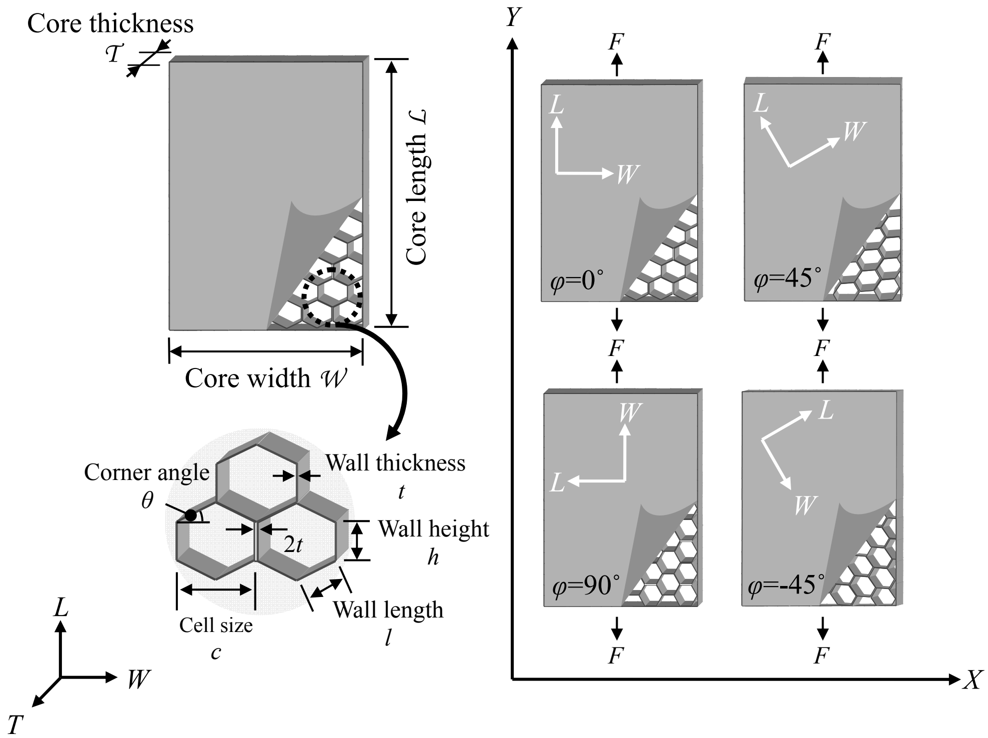

Figure 4: Geometrical parameters for the honeycomb cores and the cells. On the right side, specimen of different orientations $\varphi_1 = 0°$, $\varphi_2 = 90°$ and $\varphi_{3,4} = \pm 45°$ relative to uni-axial loading are illustrated.

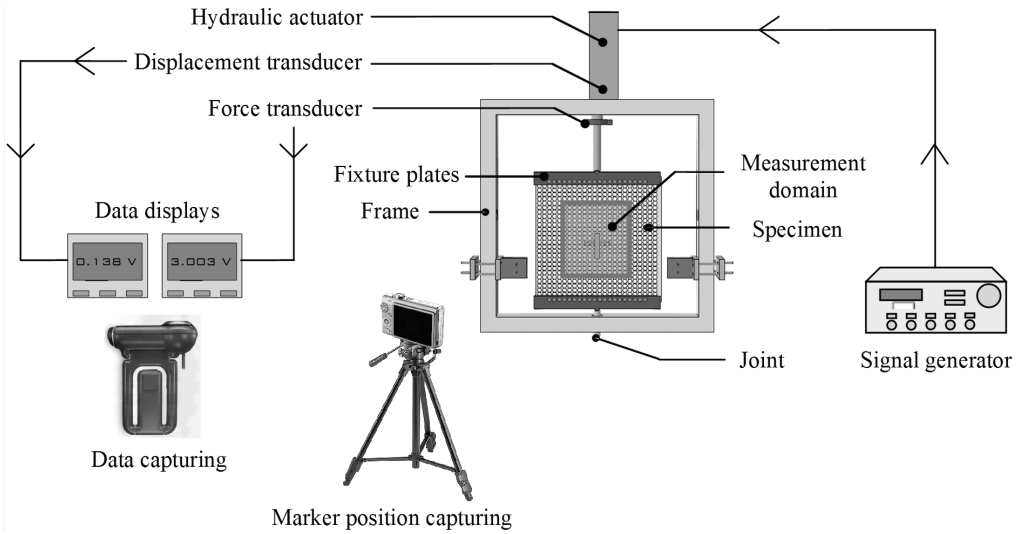

Figure 5: Uni-axial tensile test setup.

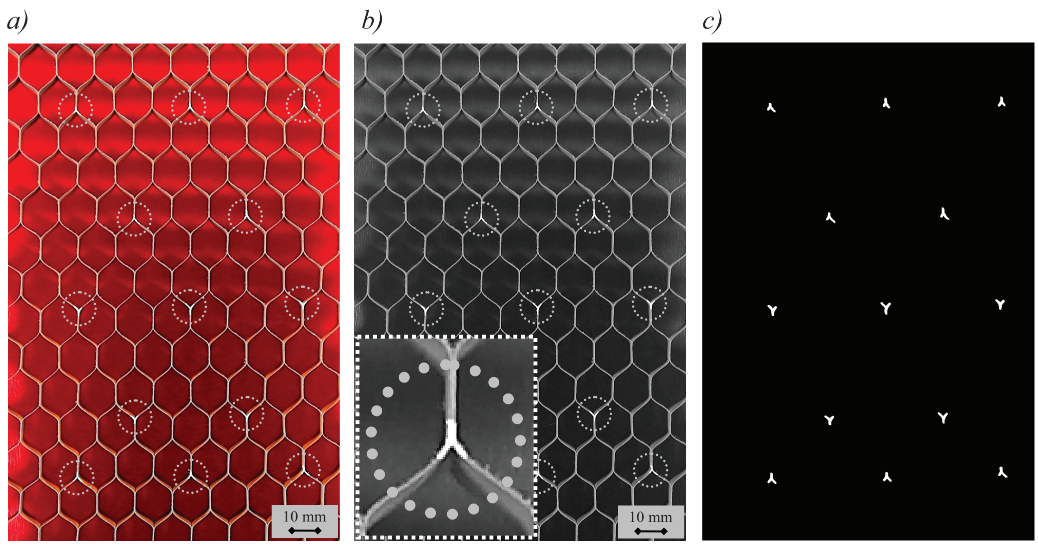

Figure 6: Marker detection in the measurement domain: a) Three-channel input image, b) Grey-scale image, c) Binary image and marker position data formation. For better visibility, markers are indicated using dashed circles.

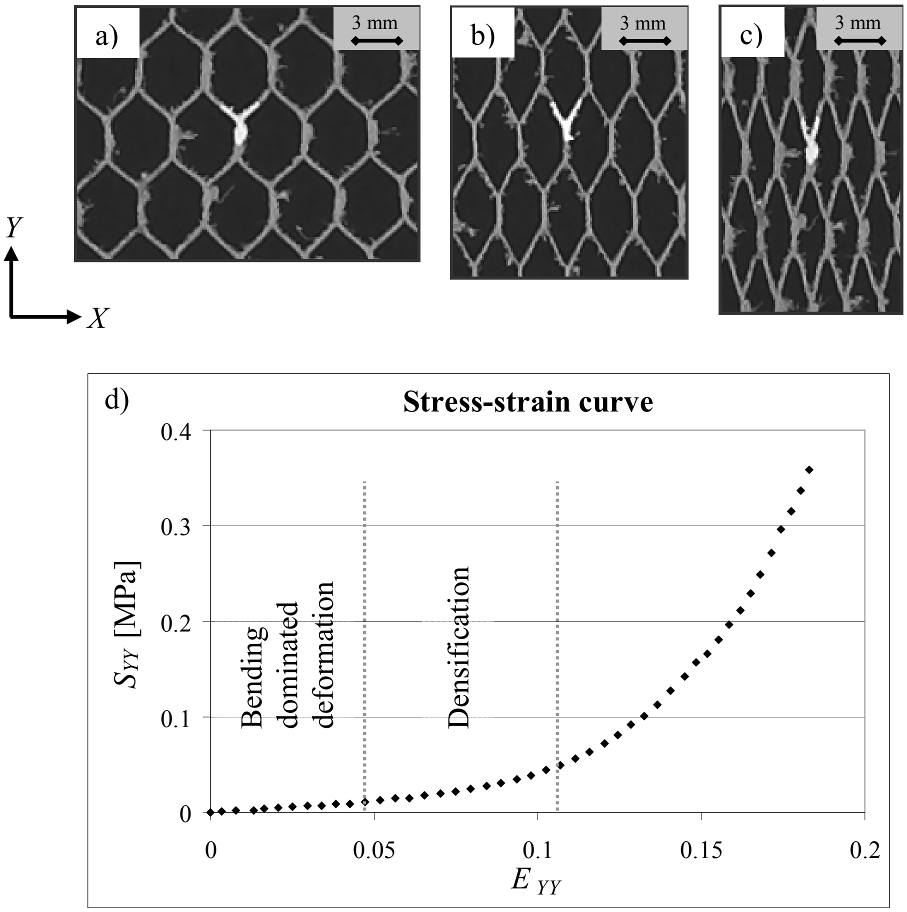

Figure 7: Deformation of Nomex® honeycomb core with cell size c=5 mm and $\varphi = 0°$: a) Undeformed structure, b) Deformation due to cell wall bending, c) Deformation during densification, d) Stress-strain curve for the core under uni-axial tensile load along Y-axis.

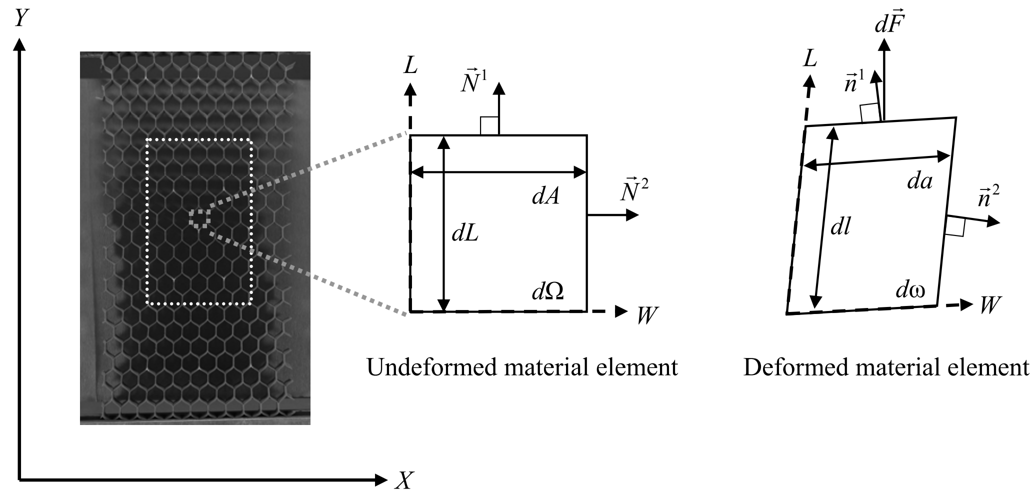

Figure 8: Infinitesimal material element in initial (left) and deformed (right) configurations. Here, $d\Omega$, dA, dL represent the material body, unit surface area and unit length in the initial configuration, respectively, while $d\omega$, da, dl are for the same parameters in deformed configuration. Surface normal vectors are denoted with $\vec{N}^i$ and $\vec{n}^i$, for which $i \in \{1, 2\}$.